

Kinematic Space and Wormholes

Jian-dong Zhang^{1*} and Bin Chen^{2,3,4†}

¹*TianQin Research Center for Gravitational Physics, Sun Yat-sen University,
Zhuhai 519082, Guangdong, P. R. China*

²*Department of Physics and State Key Laboratory of Nuclear Physics and Technology,
Peking University, Beijing 100871, P. R. China*

³*Collaborative Innovation Center of Quantum Matter, 5 Yiheyuan Rd,
Beijing 100871, P. R. China*

⁴*Center for High Energy Physics, Peking University, 5 Yiheyuan Rd,
Beijing 100871, P. R. China*

Abstract

The kinematic space could play a key role in constructing the bulk geometry from dual CFT. In this paper, we study the kinematic space from geometric points of view, without resorting to differential entropy. We find that the kinematic space could be intrinsically defined in the embedding space. For each oriented geodesic in the Poincaré disk, there is a corresponding point in the kinematic space. This point is the tip of the causal diamond of the disk whose intersection with the Poincaré disk determines the geodesic. In this geometric construction, the causal structure in the kinematic space can be seen clearly. Moreover, we find that every transformation in the $SL(2, \mathbb{R})$ leads to a geodesic in the kinematic space. In particular, for a hyperbolic transformation defining a BTZ black hole, it is a timelike geodesic in the kinematic space. We show that the horizon length of the static BTZ black hole could be computed by the geodesic length of corresponding points in the kinematic space. Furthermore, we discuss the fundamental regions in the kinematic space for the BTZ blackhole and multi-boundary wormholes.

*jdzhsfsm@gmail.com

†bchen01@pku.edu.cn

1 Introduction

One of recent developments in the AdS/CFT correspondence is on the emergence of spacetime and diffeomorphism. The key notion in the study of the emergent spacetime is the entanglement and its holographic computation. The holographic entanglement entropy in the Einstein gravity is proposed in [1, 2] to be

$$S_{RT} = \frac{A}{4G_N}, \quad (1.1)$$

where A is the area of the minimal surface which is homologous to the boundary region. This formula, being reminiscent of the Bekenstein-Hawking formula for the black hole entropy[3], suggest a deep relation between quantum gravity and quantum information. It has been widely suspected that the holographic entanglement entropy could play a pivotal role in constructing bulk spacetime and even bulk physics.

There are several proposals to construct the bulk geometry from boundary CFT, mainly based on the concept of the tensor network [4, 5, 6, 7, 8, 9, 10]. Among them, one promising approach proposed by B. Czech et.al is to view the MERA(Multi-scale Entanglement Renormalization Ansatz) tensor network as a discrete version of vacuum kinematic space[7, 8]. This proposal is inspired by the study of the hole entropy in the bulk from dual CFT data, which suggests a way to define the bulk geometry from differential entropy[11]. To compute the length of a curve γ in the hyperbolic plane, one could apply integral geometry rather than differential geometry. The length could be given by the Crofton formula

$$\text{Length of the curve } \gamma = \frac{1}{4} \int_K \omega(\theta, \alpha) n_\gamma(\theta, \alpha), \quad (1.2)$$

where θ and α label the oriented geodesic in the Poincaré disk, $n_\gamma(\theta, \alpha)$ is the intersection number of the geodesic with the curve γ and K denotes the kinematic space. The most interesting part is on the measure $\omega(\theta, \alpha)$ in the kinematic space, which has the form as

$$\omega(\theta, \alpha) = -\frac{1}{\sin^2 \alpha} \delta\alpha \wedge d\theta, \quad (1.3)$$

or in terms of the coordinates of the ending points of the geodesics on the disk boundary

$$u = \theta - \alpha, \quad v = \theta + \alpha, \quad (1.4)$$

the form of the measure becomes

$$\omega(u, v) = \frac{1}{2 \sin^2 \left(\frac{v-u}{2} \right)} du \wedge dv. \quad (1.5)$$

This measure is more suggestive when being given by

$$\omega(u, v) = \frac{\partial^2 S(u, v)}{\partial u \partial v} du \wedge dv, \quad (1.6)$$

where $S(u, v)$ is the entanglement entropy of the interval (u, v) . In [12], the authors furthermore suggest that the Crofton form should be interpreted as the conditional mutual information¹. The basic picture on the kinematic space is that it is an auxiliary Lorentzian geometry, whose metric is defined in terms of conditional mutual information.

In this paper, we would like to study the kinematic space from geometric points of view². We show that the kinematic space can be defined in a geometric way. Simply speaking, every geodesics in the Poincaré disk could define a causal cone, whose tips are in the kinematic space. The causal structure in the kinematic space can be seen clearly in this geometric picture. Moreover, we discuss the static wormhole solution in the AdS_3 gravity and its representation in the kinematic space. We show that the timelike geodesic in the kinematic space is closely related to the isometric transformation of hyperbolic type. For the BTZ spacetime formed by the identification of the geodesics with respect to a hyperbolic element in the Fuchsian group, its horizon length could be read from the timelike geodesic distance in the kinematic space between the points corresponding to the geodesics in the disk. Therefore for the eternal BTZ black hole formed by the identification of a pair of geodesics, it could be described by two timelike separated points in the kinematic space. These two points cannot be determined uniquely. As long as a pair of points lie in the timelike geodesic determined by the transformation and the geodesic distance between them is fixed, they describe the same BTZ spacetime. On the other hand, the timelike geodesic defined by a hyperbolic transformation is unique. In this sense, the BTZ spacetime could be related to a timelike geodesic in the kinematic space. In the similar spirit, we can describe the multi-boundary wormhole easily.

Another interesting issue is to consider the kinematic space for the BTZ wormhole and other multi-boundary wormhole background. The kinematic space can still be defined by the geodesics in these spacetime. We start from the kinematic space for AdS_3 , and take into account of the quotient identification defining the wormhole. We discuss carefully how to classify the geodesics in the BTZ spacetime and propose a consistent rule to define the fundamental region in the kinematic space for the BTZ spacetime. We furthermore show that the fundamental region for the multi-boundary wormhole could be defined to be the intersection of the fundamental regions for the BTZ spacetimes, each being defined by the fundamental elements of the Fuchsian group.

The remaining part of this article is organized as follows. In section 2, after giving a brief review of AdS_3 spacetime and its different coordinate systems, we show how to describe the kinematic space. In section 3, we review the construction of the static BTZ black hole and general multi-boundary wormholes by using the Fuchsian group identification. Especially we discuss the three-boundary wormhole and single-boundary torus wormhole. In section 4, we discuss the properties of the kinematic space. We show

¹For the higher dimensional study of the Crofton form and its interpretation, see [13, 14].

²While we are preparing this manuscript, there appeared two works [15, 16], which partially overlap our discussion in section 2.

that a $SL(2, R)$ transformation, being the isometric transformation of AdS_3 , define a geodesic in the kinematic space. In particular, we study the three boundary wormhole to get its fundamental regions in the kinematic space, and give a method to get the fundamental region in kinematic space for general wormholes. We end with conclusions and discussions in section 5.

2 AdS_3 and its Kinematic Space

The AdS_3 can be taken to be a hyperboloid space in the $2+2$ dimensional flat spacetime $\mathbb{R}^{2,2}$ with the metric

$$ds^2 = -dU^2 - dV^2 + dX^2 + dY^2, \quad (2.1)$$

The AdS_3 spacetime is defined by the relation

$$-U^2 - V^2 + X^2 + Y^2 = -l^2, \quad (2.2)$$

where l is the AdS radius. For simplicity, we set $l = 1$ in this paper. Defining the coordinates

$$\begin{aligned} U &= \cosh \rho \cos \tau, & V &= \cosh \rho \sin \tau, \\ X &= \sinh \rho \cos \theta, & Y &= \sinh \rho \sin \theta, \end{aligned} \quad (2.3)$$

we can read the metric of AdS_3 in the global AdS coordinates

$$\begin{aligned} ds^2 &= -\cosh^2 \rho d\tau^2 + d\rho^2 + \sinh^2 \rho d\theta^2, \\ \tau &\in \mathbb{R}, \quad \rho > 0, \quad \theta \sim \theta + 2\pi. \end{aligned} \quad (2.4)$$

The classical solutions in the AdS_3 gravity could be constructed by the quotient identification by the discrete subgroup of the isometry group $SL(2, \mathbb{R})$. If we focus on the static solutions, the construction could be understood as the identification of the geodesics pairwise in the constant time slice of AdS_3 . The constant time slice is a two-dimensional hyperboloid \mathbb{H}_2 , the so-called Poincaré upper half plane, which is of the metric

$$ds^2 = d\rho^2 + \sinh^2 \rho d\theta^2. \quad (2.5)$$

In fact, for simplicity we just take the $\tau = 0$ slice, this is equivalent to $V = 0$.

2.1 \mathbb{H}_2 and dS_2

The relation between the constant time slice of AdS_3 and the kinematic space is most easily seen by embedding them into the three-dimensional flat spacetime, which is the $V = 0$ slice of $\mathbb{R}^{2,2}$

$$ds^2 = -dU^2 + dX^2 + dY^2. \quad (2.6)$$

The two-sheeted hyperboloid \mathbb{H}_2 is then the $V = 0$ slice of AdS_3

$$U^2 - X^2 - Y^2 = 1. \quad (2.7)$$

With the embedding coordinates

$$U = \cosh \rho, \quad X = \sinh \rho \cos \theta, \quad Y = \sinh \rho \sin \theta, \quad (2.8)$$

we recover the metric (2.5). If we make a projection from the point $(U, X, Y) = (-1, 0, 0)$, we can project the upper sheet of the hyperboloid onto the unit disk

$$X^2 + Y^2 \leq 1, \quad \text{at } U = 0, \quad (2.9)$$

which is usually called the Poincaré disk. With the disk coordinates x_D, y_D , we can read the relations between the points on the hyperboloid and the disk

$$\begin{aligned} x_D &= \frac{X}{U+1} = \frac{\sinh \rho \cos \theta}{\cosh \rho + 1}, \\ y_D &= \frac{Y}{U+1} = \frac{\sinh \rho \sin \theta}{\cosh \rho + 1}. \end{aligned} \quad (2.10)$$

We may introduce the polar coordinates on the disk

$$x_D = r \cos \vartheta, \quad y_D = r \sin \vartheta. \quad (2.11)$$

Then we can solve that $\vartheta = \theta$, and get the metric of Poincaré disk

$$ds^2 = 4 \frac{dr^2 + r^2 d\vartheta^2}{1 - r^2} = 4 \frac{dx_D^2 + dy_D^2}{1 - x_D^2 - y_D^2}. \quad (2.12)$$

On the other hand, the two-dimensional de Sitter spacetime can be embedded into the same spacetime (2.6) as well. It is defined by the relation

$$X^2 + Y^2 - U^2 = 1. \quad (2.13)$$

By defining a new coordinate system with the following relation

$$U = \sinh \tau, \quad X = \cosh \tau \cos \theta, \quad Y = \cosh \tau \sin \theta, \quad (2.14)$$

we can get the metric of dS_2

$$ds^2 = -d\tau^2 + \cosh^2 \tau d\theta^2. \quad (2.15)$$

If we make another coordinate transformation

$$\cosh \tau = \frac{1}{\sin \alpha}, \quad \alpha \in (0, \pi). \quad (2.16)$$

then in terms of the coordinates (θ, α) we find another metric form of the dS_2 spacetime

$$ds^2 = \frac{-d\alpha^2 + d\theta^2}{\sin^2 \alpha}. \quad (2.17)$$

And the point (θ, α) in this coordinate will correspond to $(-\cot \alpha, \frac{\cos \theta}{\sin \alpha}, \frac{\sin \theta}{\sin \alpha})$ in (U, X, Y) coordinate.

We can define H_2 and dS_2 on the Poincaré upper half plane by introducing

$$x = \frac{X}{U - Y}, \quad y = \frac{1}{U - Y}. \quad (2.18)$$

Then the metrics of the hyperbolic space and de Sitter spacetime are respectively

$$ds^2 = \frac{dx^2 + dy^2}{y^2}, \quad \text{and} \quad ds^2 = \frac{dx^2 - dy^2}{y^2}. \quad (2.19)$$

Let us define

$$z_D = x_D + iy_D, \quad z = x + iy, \quad (2.20)$$

then the transformation between the coordinates on the Poincaré upper half plane and the ones on the Poincaré disk is

$$z = \frac{z_D + i}{iz_D + 1}, \quad z_D = \frac{iz + 1}{z + i}. \quad (2.21)$$

Or, more explicitly,

$$\begin{aligned} x &= \frac{2x_D}{x_D^2 + (1 - y_D)^2}, & y &= \frac{1 - x_D^2 - y_D^2}{x_D^2 + (1 - y_D)^2}, \\ x_D &= \frac{2x}{x^2 + (1 + y)^2}, & y_D &= \frac{x^2 + y^2 - 1}{x^2 + (1 + y)^2}. \end{aligned} \quad (2.22)$$

2.2 Geodesics in \mathbb{H}_2

The geodesics in \mathbb{H}_2 are simple. On \mathbb{H}_2 , the equation of a geodesic without orientation is

$$\tanh \rho \cos(\theta - \theta_0) = \cos \alpha_0, \quad \theta_0 \in (0, 2\pi), \quad \alpha_0 \in (0, \frac{\pi}{2}). \quad (2.23)$$

In the coordinates of $\mathbb{R}^{2,1}$, this is

$$\cos \alpha_0 U - \cos \theta_0 X - \sin \theta_0 Y = 0. \quad (2.24)$$

This is a plane crossing the origin. So for any geodesic on \mathbb{H}_2 we can find a corresponding plane crossing the origin, and the intersection curve between this plane and hyperboloid \mathbb{H}_2 is just the geodesic. The line normal to the plane and crossing the origin intersect

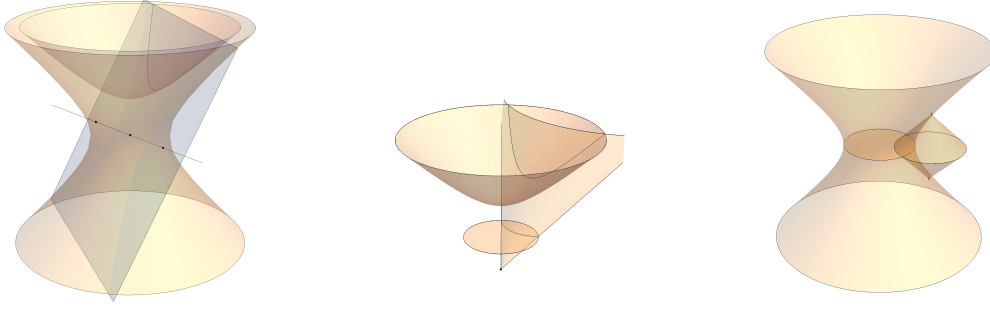


Figure 1: The upper hyperboloid is the \mathbb{H}_2 described by the embedding (2.8). The outer one-sheeted hyperboloid is the kinematic space. The unit disk in the center is the Poincaré disk. In the left figure, the plane crossing the origin intersects \mathbb{H}_2 on a curve, which is a geodesic in \mathbb{H}_2 . The line orthogonal to the plane and crossing the origin intersects the kinematic hyperboloid with two points, corresponding to the geodesics with different orientations. In the middle figure, we show the projection from the \mathbb{H}_2 hyperboloid to the Poincaré disk. The geodesic is mapped to an arc of a circle in the disk. In the right figure, we show that the the future and the past domains of dependence of the disk, whose boundary circle intersects the Poincaré disk with the arc, form a causal diamond with its tips being in the kinematic space. This gives another geometric construction of the kinematic space.

the dS_2 spacetime (2.13) at two points, as shown in the left of Fig. 1. The coordinates of these points in terms of (U, X, Y) are

$$\mp \left(\cot \alpha_0, -\frac{\cos \theta_0}{\sin \alpha_0}, -\frac{\sin \theta_0}{\sin \alpha_0} \right), \quad (2.25)$$

In terms of (θ, α) coordinate, these two points are at (θ_0, α_0) and $(\pi + \theta_0, \pi - \alpha_0)$ respectively, corresponding to the geodesics with opposite orientations. The first point correspond to geodesic starting from $\theta_0 - \alpha_0$ and ending on $\theta_0 + \alpha_0$ on the boundary, and the second point correspond to geodesic starting from $\theta_0 + \alpha_0$ and ending on $\theta_0 - \alpha_0$ on the boundary.

In the Poincare upper plane coordinate for \mathbb{H}_2 , the geodesic equation corresponding to (2.23) is

$$(\cos \alpha_0 - \sin \theta_0)(x^2 + y^2) - 2 \cos \theta_0 x + \cos \alpha_0 + \sin \theta_0 = 0. \quad (2.26)$$

It is either a semicircle or a straight line normal to the x -axis

$$\begin{cases} \text{Semicircle centered at } \left(\frac{\cos \theta_0}{\cos \alpha_0 - \sin \theta_0}, 0 \right) \text{ with radius } \left| \frac{\sin \theta_0}{\cos \alpha_0 - \sin \theta_0} \right|, & \cos \alpha_0 \neq \sin \theta_0, \\ \text{Straight line normal to the } x\text{-axis at } x = \tan \theta_0, & \cos \alpha_0 = \sin \theta_0 \end{cases} \quad (2.27)$$

In the Poincaré disk, as shown in the middle of Fig. 1, the geodesic equation corresponding to (2.23) is

$$\cos \alpha_0 (x_D^2 + y_D^2 + 1) - 2 \cos \theta_0 x_D - 2 \sin \theta_0 y_D = 0, \quad (2.28)$$

The geodesic is either an arc of a circle which is orthogonal to the unit circle when $\alpha_0 \neq \frac{\pi}{2}$, or a line crossing the origin when $\alpha_0 = 0$.

The geometric meaning of α_0 and θ_0 is clear: α_0 is the opening angle of the arc of the unit circle intersected by the geodesic, and θ_0 is the angular coordinate of the midpoint of this arc. In the disk, we can also denote each geodesic by the angular coordinates (μ, ν) of its two endpoints on the unit circle, then we may have

$$\mu = \theta_0 - \alpha_0, \quad \nu = \theta_0 + \alpha_0, \quad (2.29)$$

to define the kinematic space[12]. We should notice that in the kinematic space the points (θ_0, α_0) and $(\theta_0 + \pi, \pi - \alpha_0)$ denote the same geodesic but with different orientations. Remarkably, the kinematic space is exactly the dS_2 spacetime (2.17) with the coordinates (θ, α) and the metric (2.17) given above. Therefore we can conclude that the dS_2 spacetime defined by (2.13) is exactly the kinematic space of \mathbb{H}_2 .

In the above discussion, we have the picture that the corresponding points of a geodesic in the kinematic space are the same as the points we get on dS_2 in Eq. (2.25) by the intersection of the normal line to the plane (2.24). This picture shows explicitly the relation between a hyperbolic space and its kinematic space³. However, in the kinematic space, the points could be timelike or spacelike separated, depending on whether the corresponding geodesics have intersection or not[7]. It is not clear to see why there exist such a kind of relations in the above construction.

There is another geometric construction to show the causal relation of the points in the kinematic space more clearly. As we shown above, the geodesic (2.26) in the Poincaré disk is actually part of a circle. This circle is the boundary of a disk, which in general is not of unit radius. The interesting point is that the future and the past domains of dependence of this disk form a causal diamond with its tips being actually in the kinematic space, as showed in the right figure of Fig. 1. In the embedding space, the coordinates of the tips are

$$\left(\pm \tan \alpha_0, \frac{\cos \theta_0}{\cos \alpha_0}, \frac{\sin \theta_0}{\cos \alpha_0} \right), \quad (2.30)$$

while in the kinematic space, their corresponding coordinates $(\tilde{\theta}, \tilde{\alpha})$ satisfy the relation

$$\tilde{\theta} = \theta_0, \quad \tilde{\alpha} = \frac{\pi}{2} \pm \alpha_0. \quad (2.31)$$

³This has already been pointed out in Fig. 15 in [12].

They are slightly different from the points (θ_0, α_0) or $(\theta_0 + \pi, \pi - \alpha_0)$ corresponding to the geodesic by using the normal line.

However, the difference is just a constant translation. It is the same as the kinematic space. Therefore, we can safely take the tips of the diamond as the points corresponding to the geodesic.

This picture has the advantage to see the causal structure clearly. For example, in the Poincaré disk, if two geodesics have no intersection but have the same orientation, then the casual diamond of the outer geodesics encloses the one of the inner geodesics, such that the corresponding point of the inner geodesic is at the casual past of the one of the outer geodesic. This shows that the causal relation can be seen directly from the embedding picture by the relation of the corresponding light cone. If the causal diamond of two geodesic has no intersection, the corresponding geodesics have no intersection as well. And if two causal diamond have intersection, then the geodesics will also have intersection.

Moreover, in the first picture, we must decide the embedded dS_2 surface first, then we can get the corresponding point. But in the second picture, we do not need to know the surface of kinematic space. We can directly get corresponding points of all geodesics, which form the kinematic space. And then we can get the induced metric on this surface, and this is exactly the metric of the kinematic space.

3 Symmetries on AdS_3 and its quotients

Every classical solution in the AdS_3 graviy is locally AdS_3 . They could be constructed by the quotient identification of global AdS_3 . For example, the BTZ geometry is a quotient of AdS_3 by a discrete subgroup of $PSL(2, \mathbb{R})$ [17, 18]. It is a two-boundary wormhole, or an eternal black hole[19].

More interesting, there exist many different kinds of multi-boundary wormholes with different topology. For the static spacetime, one may identify the geodesics in the Poincaré disk to construct such multi-boundary wormholes. The detailed construction could be found in [20, 21, 22, 23, 24, 25]. In this section, we will give a brief review of these solutions and discuss three examples carefully, they are BTZ, three-boundary wormhole and single-boundary torus wormhole.

3.1 Fuchsian group and its action

In this subsection, let us focus on the symmetry transformation on the constant time slice of AdS_3 . For simplicity, we start from the Poincaré upper plane. The symmetry group is $PSL(2, \mathbb{R}) = SL(2, \mathbb{R})/\{\pm 1\}$, which could be represented by a matrix

$$\gamma = \begin{pmatrix} a & b \\ c & d \end{pmatrix}, \quad (3.1)$$

with $|\gamma| = ad - bc = 1$, $a, b, c, d \in \mathbb{R}$. We require the transformation to be hyperbolic to avoid the orbifold singularities. This requirement leads to $|\text{Tr}\gamma| = |a + d| > 2$, which defines the Fuchsian group of the second kind. On the half plane, we have the complex coordinate $z = x + iy$. A point $z = x + iy$ is transformed into $z' = x' + iy' = \gamma z$ under the Mobius transformation γ

$$z' = \frac{az + b}{cz + d}. \quad (3.2)$$

Such a transformation leads to a Riemann surface $\Sigma = \mathbb{H}_2/\Gamma$, where Γ is a discrete subgroup which is called the Fuchsian group and is generated by its fundamental element γ as $\Gamma = \{\gamma^n | n \in \mathbb{Z}\}$.

For each transformation, we also have an one-parameter family of flow lines

$$f(x, y) = cx^2 + (d - a)x + cy^2 + ey - b = 0, \quad e \in \mathbb{R}. \quad (3.3)$$

These flow lines are the integral curve of the transformation. Every flow line is a circle which crosses the two fixed points of the transformation on the boundary $y = 0$, and $x = \frac{a-d \pm \sqrt{(a+d)^2 - 4}}{2c}$. When $e = 0$, the flow line becomes a geodesic in H_2 , and we call it the geodesic flow line. For every point z , we can find a e such that the point locates on the corresponding flow line, then the point γz locates on the same flow line as well.

Under a transformation γ , a geodesic $(x - x_0)^2 + y^2 = r^2$ changes to another geodesic $(x - x'_0)^2 + y^2 = r'^2$ with the parameters being

$$\begin{aligned} x'_0 &= \frac{ac(x_0^2 - r^2) + (ad + bc)x_0 + bd}{(cx_0 + d)^2 - c^2r^2}, \\ r'^2 &= \frac{r^2}{((cx_0 + d)^2 - c^2r^2)^2}. \end{aligned} \quad (3.4)$$

Given two geodesics, the transformation relating them to each other is not unique. If a geodesic is normal to every flow lines of a transformation, then it is called an eigen-geodesic of the transformation. Given two geodesics without intersection, there exist many transformation that can transform one to another. But there exist a unique transformation such that both geodesics are the eigen-geodesics of this transformation.

The discussion is similar in the Poincaré disk. As shown in Fig. 2, among the flow lines intersecting with the geodesics, the geodesic flow line is special. Actually, the distance between the points of two geodesics is the shortest along the geodesic flow line. Such a distance is defined to be the distance of two geodesics.

3.2 BTZ black hole as quotient

The black hole could be taken as the quotient of the global AdS_3 by a discrete group of $PSL(2, \mathbb{R})$. The action could be seen most easily in the Poincaré disk, if we are only interested in the static configuration. In fact, if we want to get a BTZ black hole,

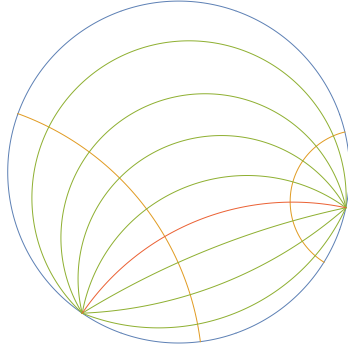


Figure 2: The unit disk inside the blue circle is the Poincaré disk. The two orange arcs are the eigen-geodesics of a $PSL(2, R)$ transformation. The green and red arcs are the flow lines of this transformation, and they are normal to the two geodesics. The intersection point of one geodesic with a flow line is transformed into the intersection point of the other geodesic with the same flow line. Especially, the red arc is the geodesic flow line. The length of the arc between two intersection points of the geodesics with the geodesic flow line is the distance between two geodesics.

we should start from a Fuchsian group defined by $\Gamma = \{\gamma^n | \gamma \in PSL(2, \mathbb{R}), n \in \mathbb{Z}\}$, where γ is the fundamental element such that the group is denoted as $\Gamma = \{\gamma\}$. On the disk, we can choose a pair of non-intersecting geodesics to be identified by this element. Such identification can be extended to AdS_3 and leads to a static BTZ black hole. The horizon length of the BTZ black hole L_H can be computed directly by [26]

$$|\text{Tr} \gamma| = 2 \cosh \frac{L_H}{2}. \quad (3.5)$$

The group $\{\gamma\}$ and $\{M^{-1}\gamma M\}$ represent the same BTZ black hole. And the flow line of the fundamental element represents the angle direction of the black hole, while the eigen-geodesics represents the radius direction.

As the transformations with the same trace correspond to the same BTZ, we can start from the simplest case with the fundamental element being of a diagonal form

$$\gamma = \begin{pmatrix} \lambda & 0 \\ 0 & \frac{1}{\lambda} \end{pmatrix}, \quad (3.6)$$

such that the transformation is just $\gamma z = \lambda^2 z$. Without losing generality, we can assume $\lambda > 1$. Then its flow line is $y = kx$, and one of its eigen-geodesics is $\mathbf{L}_1 : x^2 + y^2 = r^2$. Under the fundamental transformation, the eigen-geodesic is transformed into $\mathbf{L}_2 = \gamma \mathbf{L}_1 : x^2 + y^2 = \lambda^4 r^2$. The identification of L_1 and L_2 leads to the black hole. There is still an ambiguity in choosing the value of r , which does not change the following discussion. The geodesic flow line is $x = 0$, and it intersects the two geodesics at the

points $(0, r)$, $(0, \lambda^2 r)$. Therefore the length between two geodesics is

$$L_H = \int_r^{\lambda^2 r} \frac{dy}{y} = 2 \ln \lambda, \quad (3.7)$$

which is independent of the value of r . It is easy to check that the length obeys the relation

$$2 \cosh \frac{L_H}{2} = 2 \cosh \ln \lambda = \lambda + \frac{1}{\lambda} = \text{Tr} \gamma. \quad (3.8)$$

For a general element γ , we can always find a transformation M such that $\gamma' = M^{-1} \gamma M$ is diagonal

$$\gamma = \begin{pmatrix} a & b \\ c & d \end{pmatrix}, \quad \gamma' = \begin{pmatrix} \lambda & 0 \\ 0 & \frac{1}{\lambda} \end{pmatrix}, \quad M = \begin{pmatrix} \zeta_A & \zeta_B \\ 1 & 1 \end{pmatrix} \quad (3.9)$$

where the parameters are

$$\begin{aligned} \lambda &= \frac{1}{2}(a + d + \sqrt{(a + d)^2 - 4}), & \frac{1}{\lambda} &= \frac{1}{2}(a + d - \sqrt{(a + d)^2 - 4}), \\ \zeta_A &= \frac{1}{2c}(a - d + \sqrt{(a + d)^2 - 4}), & \zeta_B &= \frac{1}{2c}(a - d - \sqrt{(a + d)^2 - 4}). \end{aligned} \quad (3.10)$$

If γ is hyperbolic, then we will have $|a + d| > 2$, and the above parameters are all real. Now ζ_A and ζ_B are the coordinates of the two fixed points of γ on the boundary for hyperbolic γ .

For parabolic or elliptic γ , $\zeta_{A,B}$ are not real numbers, and the fixed points are at $(\frac{a-d}{2c}, \pm \frac{\sqrt{4-(a+d)^2}}{2c})$. In these cases, the flow lines are the circles around the fixed points, and the eigen-geodesics are the geodesics starting and ending at the fixed points.

The eigen-geodesic of a hyperbolic γ' and its image under the transformation

$$\mathbf{L}'_1 : x^2 + y^2 = r^2, \quad \mathbf{L}'_2 = \gamma' \mathbf{L}'_1 : x^2 + y^2 = \lambda^4 r^2, \quad (3.11)$$

can be mapped into the eigen-geodesics of γ by

$$\mathbf{L}_1 = M \mathbf{L}'_1, \quad \mathbf{L}_2 = \gamma \mathbf{L}_1 = M \gamma' M^{-1} M \mathbf{L}'_1 = M \mathbf{L}'_2. \quad (3.12)$$

The explicit forms of the eigen-geodesics are

$$\begin{aligned} \mathbf{L}_1 : \quad & \left(x - \frac{\zeta_A r^2 - \zeta_B}{r^2 - 1} \right)^2 + y^2 = \frac{(\zeta_A - \zeta_B)^2 r^2}{(r^2 - 1)^2}, \\ \mathbf{L}_2 : \quad & \left(x - \frac{\zeta_A \lambda^4 r^2 - \zeta_B}{\lambda^4 r^2 - 1} \right)^2 + y^2 = \frac{(\zeta_A - \zeta_B)^2 \lambda^4 r^2}{(\lambda^4 r^2 - 1)^2}. \end{aligned} \quad (3.13)$$

For a elliptic or parabolic γ , its eigen-geodesics $(x - x_0)^2 + y^2 = r_0^2$ should satisfy

$$r_0^2 = \left(\frac{a-d}{2c} - x_0 \right)^2 + \frac{4 - (a+d)^2}{4c^2} = x_0^2 + \frac{a-d}{c} x_0 + \frac{1-ad}{c^2} \quad (3.14)$$

We can compute the distance of any two geodesics described by

$$(x - x_1)^2 + y^2 = r_1^2, \quad (x - x_2)^2 + y^2 = r_2^2, \quad r_1, r_2 > 0. \quad (3.15)$$

The four end points of two geodesics at $y = 0$ are $u_1 = x_1 - r_1$, $v_1 = x_1 + r_1$, $u_2 = x_2 - r_2$, $v_2 = x_2 + r_2$ respectively. We always have $u_1 < v_1$, $u_2 < v_2$, and without losing generality we assume that $v_1 < v_2$. We require that the two geodesics have no intersection, which include two possibilities:

$$\begin{aligned} \text{Case I:} \quad & u_1 < v_1 < u_2 < v_2, \\ \text{Case II:} \quad & u_2 < u_1 < v_1 < v_2. \end{aligned} \quad (3.16)$$

In the case I the two circles looks independent, while in the case II the first circle with the radius r_1 is enclosed by the second circle with the radius r_2 . For convenience, we introduce three parameters

$$A = (u_1 - u_2)(v_1 - v_2), \quad B = (u_1 - v_2)(v_1 - u_2), \quad C = (u_1 - v_1)(u_2 - v_2). \quad (3.17)$$

Then in the case I we have $A, B > 0$, and in the case II we have $A, B < 0$. In both cases, we always find $C = A - B > 0$. The distance between two geodesics or the horizon length of the resulting BTZ black hole can be computed straightforwardly. It is determined by the trace of the element γ . For the above two cases, we find

$$\begin{aligned} I : \quad \text{Tr} \gamma &= 2\sqrt{\frac{A}{C}}, & L_H &= 2 \ln \left(\sqrt{\frac{A}{C}} + \sqrt{\frac{B}{C}} \right), \\ II : \quad \text{Tr} \gamma &= 2\sqrt{-\frac{B}{C}}, & L_H &= 2 \ln \left(\sqrt{-\frac{B}{C}} + \sqrt{-\frac{A}{C}} \right). \end{aligned} \quad (3.18)$$

This result can be written in an uniform way

$$L_H = 2 \ln \left(\sqrt{\frac{|A|}{C}} + \sqrt{\frac{|B|}{C}} \right) \quad (3.19)$$

The above discussion can be translated into the language in the Poincaré disk easily. Now in terms of the polar coordinates $x_D = r \cos \theta$, $y_D = r \sin \theta$, the metric of the disc is of the form

$$ds^2 = 4 \frac{dr^2 + r^2 d\theta^2}{(1 - r^2)^2}. \quad (3.20)$$

The unit circle $r = 1$ is the boundary of the disk, corresponding to the boundary of H_2 . The points on the circle is parameterized by the angular coordinate θ . The point $(x, 0)$ on the boundary of the upper half plane is mapped to the point $(1, \theta)$ with

$$\theta = 2 \arctan x - \frac{\pi}{2}, \quad \theta \in \left(-\frac{3\pi}{2}, \frac{\pi}{2}\right). \quad (3.21)$$

Every geodesic in the disk can be characterized by the angular coordinates of its ending points (μ, ν) , $\mu < \nu$, or equivalently in terms of the coordinates in the kinematic space $(\theta = \frac{\mu+\nu}{2}, \alpha = \frac{\nu-\mu}{2})$. For two geodesics (μ_1, ν_1) , (μ_2, ν_2) in the disk, the distance between them is just

$$L_H = 2 \ln \frac{\sqrt{|\cos(\alpha_1 - \alpha_2) - \cos(\theta_1 - \theta_2)|} + \sqrt{|\cos(\alpha_1 + \alpha_2) - \cos(\theta_1 - \theta_2)|}}{\sqrt{2 \sin \alpha_1 \sin \alpha_2}} \quad (3.22)$$

One subtle point is that each geodesic actually corresponds to two points in the kinematic space, depending on the orientation. The points (θ, α) and $(\theta + \pi, \pi - \alpha)$ correspond to the same geodesic if we disregard its orientation. If two points (θ_1, α_1) and (θ_2, α_2) are timelike separated, then the points (θ_1, α_1) and $(\theta_2 + \pi, \pi - \alpha_2)$ must be spacelike separated. The distance (3.22) between two geodesics is insensitive to the relative orientation of the geodesics. However, in order to construct the BTZ black hole by identifying the geodesics in pair, the geodesics should have the right orientations. Correspondingly the points in the kinematic space must be timelike separated. If two points in the kinematic space are timelike separated, then their corresponding geodesics contain each other, have no intersection and have the same orientation. If they are null separated, then their corresponding geodesics have one common endpoint. And if two points are spacelike separated, then their corresponding geodesics either have intersection or have different orientation without intersection.

3.3 Multi-boundary wormhole

For the multi-boundary wormhole, the construction is similar. Now we need more pairs of non-intersecting geodesics in the disk. Here for simplicity, we focus on the case with two pairs of geodesics. With four geodesics, there exist two kinds of identification, leading to a three-boundary wormhole and a single-boundary wormhole with the torus behind the horizon respectively. There are two fundamental elements γ_1, γ_2 for the Fuchsian group $\Gamma = \{\gamma_1, \gamma_2\}$. The corresponding gravitational configuration is denoted as AdS_3/Γ .

If the geodesic flow lines of the two fundamental elements do not intersect each other, we obtain a three-boundary wormhole. This wormhole have three asymptotic boundaries, each of which there exists a black hole. Outside every black hole's horizon, the spacetime is described exactly by the BTZ metric. In other words, the observer at the asymptotic infinity of each boundary sees a BTZ black hole. Inside the horizons, the three boundaries are connected by a region with topology of a pair of pants. The three-boundary wormhole could be characterized by the horizon lengths L_i defined on each boundary. The horizon lengths for the first two boundaries L_i are given by the γ_i : $|\text{Tr}(\gamma_i)| = 2 \cosh \frac{L_i}{2}, i = 1, 2$, and the horizon length for the third boundary is determined by $\gamma_3 = \gamma_1 \gamma_2^{-1}$. For simplicity, we can always choose the geodesic flow lines

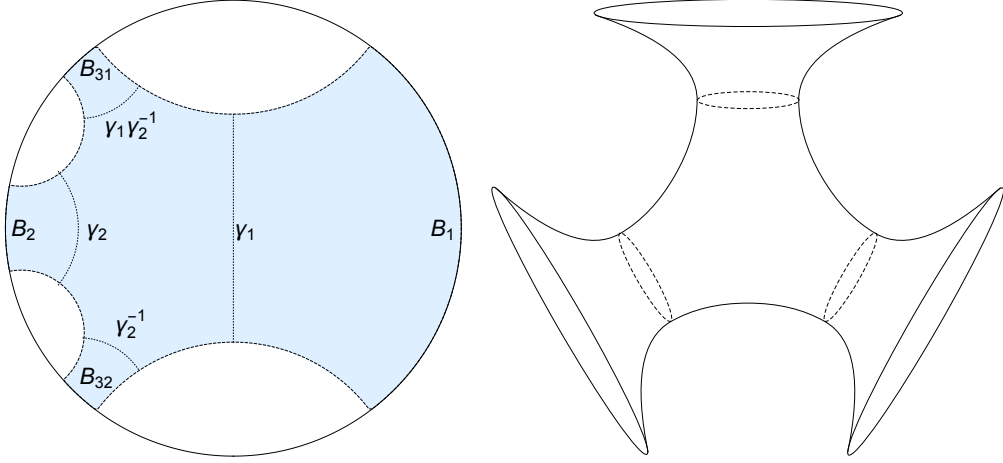


Figure 3: The three-boundary wormhole is formed by the identification of two pairs of geodesics. The figure on the left shows the fundamental region of three-boundary wormhole. The dashed lines ending on the unit circles are geodesics. B_1 and B_2 denote the first two boundaries, corresponding to the transformation γ_1 and γ_2 . B_{31} and B_{32} denote the two parts of the third boundary, which corresponds to the transformation $\gamma_1\gamma_2^{-1}$ or $\gamma_2^{-1}\gamma_1$. And the dotted lines are the corresponding horizons. The figure on the right shows the topology of the $t = 0$ slice of three boundary wormhole. The dashed lines on the right figure are the horizons of the black holes at each boundary.

of both transformations γ_1 and γ_2 to be symmetric about the x -axis on the disc. The fundamental region in the disk and the $t = 0$ slice are shown in Fig. 3. Moreover, we can also choose the transformation matrix of γ_1 to be diagonal. Then we can assume the transformation matrices are of the form

$$\gamma_1 = \begin{pmatrix} \lambda & 0 \\ 0 & \frac{1}{\lambda} \end{pmatrix}, \quad \gamma_2 = \frac{1}{2} \begin{pmatrix} \left(\mu + \frac{1}{\mu}\right) + e^\alpha \left(\mu - \frac{1}{\mu}\right) & \sqrt{e^{2\alpha} - 1} \left(\mu - \frac{1}{\mu}\right) \\ \sqrt{e^{2\alpha} - 1} \left(\mu - \frac{1}{\mu}\right) & \left(\mu + \frac{1}{\mu}\right) - e^\alpha \left(\mu - \frac{1}{\mu}\right) \end{pmatrix}, \quad (3.23)$$

with $\lambda, \mu > 1$. The horizon lengths of the black holes on the first two boundaries are respectively

$$L_1 = 2 \ln \lambda, \quad L_2 = 2 \ln \mu. \quad (3.24)$$

And the horizon length of the black hole on the third boundary L_3 is given by

$$\begin{aligned} \cosh \frac{L_3}{2} &= \frac{1}{4} \left(\lambda + \frac{1}{\lambda} \right) \left(\mu + \frac{1}{\mu} \right) - \frac{e^\alpha}{4} \left(\lambda - \frac{1}{\lambda} \right) \left(\mu - \frac{1}{\mu} \right) \\ &= \cosh \frac{L_1}{2} \cosh \frac{L_2}{2} - e^\alpha \sinh \frac{L_1}{2} \sinh \frac{L_2}{2}, \end{aligned} \quad (3.25)$$

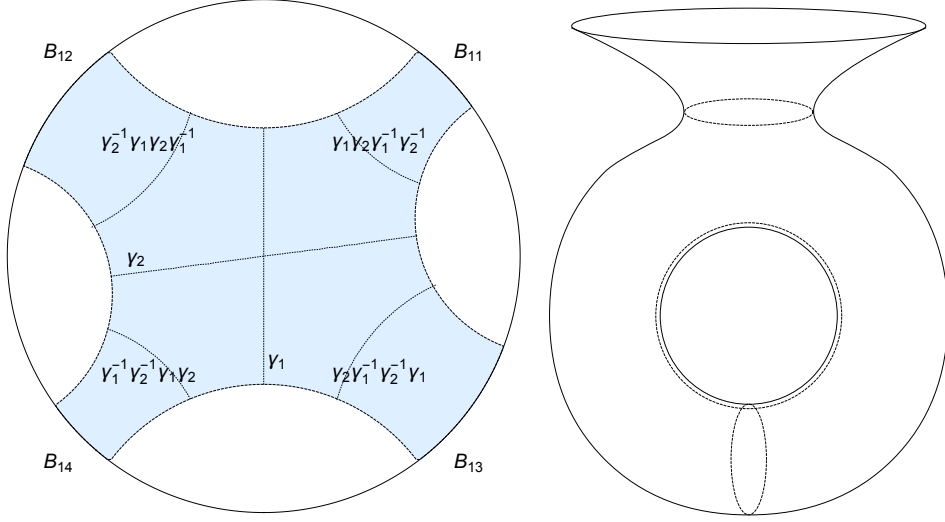


Figure 4: The torus wormhole is also given by the identification of two pairs of geodesics, which the flow lines of two fundamental elements γ_1 and γ_2 have a intersection. The figure on the left shows the fundamental region of the torus wormhole. The identifications γ_1 and γ_2 leads to two length L_1 and L_2 , which determines the shape of the torus. B_{11} , B_{12} , B_{13} , B_{14} denote the four parts of the boundary. They correspond to the transformations $\gamma_1 \gamma_2 \gamma_1^{-1} \gamma_2^{-1}$, $\gamma_2^{-1} \gamma_1 \gamma_2 \gamma_1^{-1}$, $\gamma_1^{-1} \gamma_2^{-1} \gamma_1 \gamma_2$, $\gamma_2 \gamma_1^{-1} \gamma_2^{-1} \gamma_1$. These transformations are similar to each other such that they give the asymptotic boundary of the wormhole. The figure on the right shows the topology of the $t = 0$ slice of torus wormhole. The three dashed lines include the horizon of the black hole and two cycles with length L_1, L_2 that determine the region inside the horizon.

Obviously the length L_3 depends on the real parameter α , which is restricted by

$$e^\alpha < \frac{1}{2} \left(\frac{\tanh \frac{L_1}{4}}{\tanh \frac{L_2}{4}} + \frac{\tanh \frac{L_2}{4}}{\tanh \frac{L_1}{4}} \right). \quad (3.26)$$

For the torus wormhole, we can choose the geodesic flow lines of both transformations γ_1, γ_2 to be the straight lines on the disc, say the flow line of γ_1 being $x_D = 0$, the one of γ_2 being $y_D = x_D \tan \theta$. The fundamental region in the disk and the $t = 0$ slice are shown in Fig. 4. The torus wormhole could also be characterized by three parameters, two of them being related to the length L_i defined by the γ_i : $|\text{Tr}(\gamma_i)| = 2 \cosh \frac{L_i}{2}, i = 1, 2$ and the other being the horizon length of the black hole defined by $\gamma_3 = \gamma_1^{-1} \gamma_2^{-1} \gamma_1 \gamma_2$. We may set

$$\gamma_1 = \begin{pmatrix} \lambda & 0 \\ 0 & \frac{1}{\lambda} \end{pmatrix}, \quad \gamma_2 = \frac{1}{2} \begin{pmatrix} \mu + \frac{1}{\mu} + \left(\mu - \frac{1}{\mu} \right) \sin \theta & \left(\mu - \frac{1}{\mu} \right) \cos \theta \\ \left(\mu - \frac{1}{\mu} \right) \cos \theta & \mu + \frac{1}{\mu} - \left(\mu - \frac{1}{\mu} \right) \sin \theta \end{pmatrix}, \quad (3.27)$$

and correspondingly

$$L_1 = 2 \ln \lambda, \quad L_2 = 2 \ln \mu. \quad (3.28)$$

Here the L_1 and L_2 characterize the torus in the black hole. The horizon of the black hole is determined by the element γ_3 , and the horizon length for the torus wormhole is just

$$L_H = 2 \operatorname{arccosh} \left[\frac{1}{8} \left(\lambda - \frac{1}{\lambda} \right)^2 \left(\mu - \frac{1}{\mu} \right)^2 \cos^2 \theta - 1 \right],$$

with $\left(\lambda - \frac{1}{\lambda} \right) \left(\mu - \frac{1}{\mu} \right) \cos \theta > 4.$ (3.29)

4 Kinematic space and wormhole

In section 2, we introduced the kinematic space from a geometric point of view. In this section, we study the properties of the kinematic space. We discuss the geodesics in the kinematic space and show that the geodesic distance between two time-like point is equal to the horizon length of corresponding BTZ black hole. We also show that the eigen-geodesics of a given $SL(2, \mathbb{R})$ transformation form a geodesic in the kinematic space. Furthermore we discuss the kinematic space of the wormholes, including the BTZ wormhole and multi-boundary wormholes.

4.1 Geodesics in the kinematic space

The kinematic space dS_2 could be described by the upper half plane (x, y) , $y \geq 0$ with the metric

$$ds^2 = \frac{-dy^2 + dx^2}{y^2}. \quad (4.1)$$

The geodesics in it are of three types

$$\begin{aligned} \text{timelike:} & \quad (x - x_0)^2 - y^2 = R^2, \\ \text{null:} & \quad (x - x_0)^2 - y^2 = 0, \\ \text{spacelike:} & \quad (x - x_0)^2 - y^2 = -R^2. \end{aligned} \quad (4.2)$$

On the other hand, the kinematic space can be described in terms of the coordinates (θ, α) with the metric (2.17). Then the geodesics are described by

$$\cos \alpha = A \cos(\theta - \theta_0), \quad (4.3)$$

where

$$\begin{cases} |A| > 1, & \text{timelike geodesic} \\ |A| = 1, & \text{null geodesic} \\ |A| < 1, & \text{spacelike geodesic} \end{cases} \quad (4.4)$$

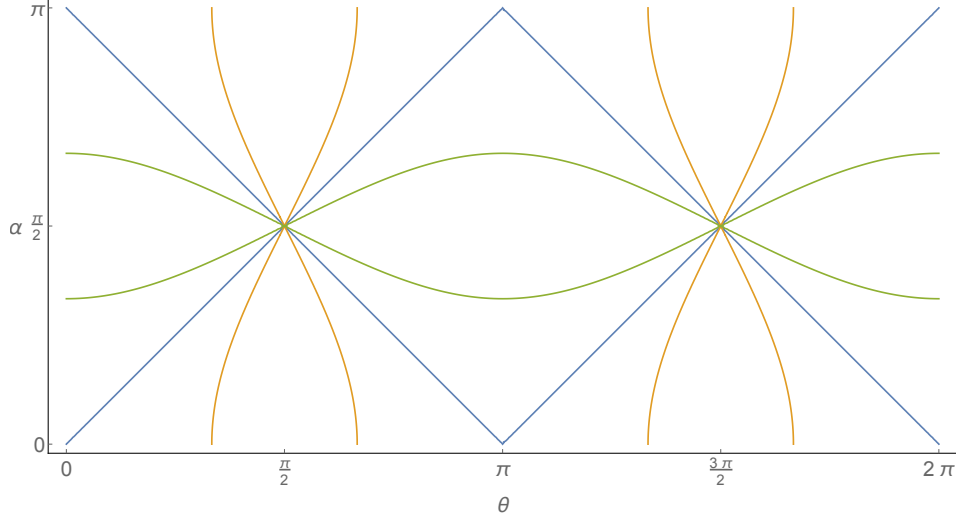


Figure 5: The geodesics in the kinematic space. The value of θ_0 for these geodesics is taken to be 0. The orange lines are the timelike geodesics with $A = \pm 2$. The blue lines are the null geodesics with $A = \pm 1$. The green lines are the spacelike geodesics with $A = \pm \frac{1}{2}$.

or

$$\theta = \theta_0, \quad (4.5)$$

which represents a timelike geodesic. In Fig. 5, we have drawn the different geodesics in the kinematic space.

For any two timelike separated points (α_1, θ_1) , (α_2, θ_2) , the geodesic connecting them has the parameters

$$\begin{aligned} A^2 &= \frac{\cos^2 \alpha_1 + \cos^2 \alpha_2 - 2 \cos \alpha_1 \cos \alpha_2 \cos(\theta_1 - \theta_2)}{\sin^2(\theta_1 - \theta_2)}, \\ A \cos \theta_0 &= \frac{\cos \alpha_2 \sin \theta_1 - \cos \alpha_1 \sin \theta_2}{\sin(\theta_1 - \theta_2)}. \end{aligned} \quad (4.6)$$

Now the nature of the geodesic could be equivalently determined by the quantity $\left| \frac{\alpha_2 - \alpha_1}{\theta_2 - \theta_1} \right|$ instead of A^2 . When this quantity is greater than 1, the geodesic is timelike, and when it is less than 1 or equals 1, the corresponding geodesic is spacelike or null respectively.

The proper time between the two points along the timelike geodesic is

$$\begin{aligned}
\Delta\tau &= \int_{\tau_1}^{\tau_2} d\tau = \int_{\alpha_1}^{\alpha_2} \frac{d\alpha}{\sin \alpha} \sqrt{1 - \left(\frac{d\theta}{d\alpha}\right)^2} \\
&= \operatorname{arctanh} \frac{\sqrt{A^2 - 1} \cos \alpha_1}{\sqrt{A^2 - \cos^2 \alpha_1}} - \operatorname{arctanh} \frac{\sqrt{A^2 - 1} \cos \alpha_2}{\sqrt{A^2 - \cos^2 \alpha_2}} \\
&= \operatorname{arctanh} \frac{\sqrt{\cos^2 \alpha_1 + \cos^2 \alpha_2 - 2 \cos \alpha_1 \cos \alpha_2 \cos(\theta_1 - \theta_2) - \sin^2(\theta_1 - \theta_2) \cos \alpha_1}}{|\cos(\theta_1 - \theta_2) \cos \alpha_1 - \cos \alpha_2|} \\
&\quad - \operatorname{arctanh} \frac{\sqrt{\cos^2 \alpha_1 + \cos^2 \alpha_2 - 2 \cos \alpha_1 \cos \alpha_2 \cos(\theta_1 - \theta_2) - \sin^2(\theta_1 - \theta_2) \cos \alpha_2}}{|\cos(\theta_1 - \theta_2) \cos \alpha_2 - \cos \alpha_1|}
\end{aligned} \tag{4.7}$$

This is exactly the distance between two geodesics which should be identified to obtain the BTZ black hole. Although it seems that (4.7) and (3.22) have very different form, they can be proved to be equal, i.e.

$$\Delta\tau \equiv L_H \tag{4.8}$$

Therefore we arrive the picture that the length of the horizon of the BTZ black hole can be read from the geodesic distance of the two time-like separated points in the kinematic space, where the two points correspond to the geodesics to be identified in the Poincaré disk.

4.2 Symmetry transformation and kinematic space geodesic

More interestingly, a given isometric transformation defines a geodesic in the kinematic space. Let us consider a hyperbolic transformation

$$\gamma = \begin{pmatrix} a & b \\ c & d \end{pmatrix}, \tag{4.9}$$

whose eigen-geodesics in the Poincaré upper half plane can be parameterized by r_0 and are given by

$$(x - x_P)^2 + y^2 = r_P^2, \tag{4.10}$$

with

$$x_P = \frac{\zeta_A r_0^2 - \zeta_B}{r_0^2 - 1}, \quad r_P = \left| \frac{(\zeta_A - \zeta_B) r_0}{(r_0^2 - 1)} \right|, \tag{4.11}$$

where ζ_A, ζ_B are elements in the matrix M defined in (3.10). In the disk, the eigen-geodesics are given by

$$x^2 - 2x_D x + y^2 - 2y_D y + 1 = 0, \tag{4.12}$$

where

$$\begin{aligned} x_D &= \frac{2x_P}{x_P^2 - r_P^2 + 1} = \frac{2(\zeta_A r_0^2 - \zeta_B)}{(\zeta_A^2 + 1)r_0^2 - (\zeta_B^2 + 1)}, \\ y_D &= \frac{x_P^2 - r_P^2 - 1}{x_P^2 - r_P^2 + 1} = \frac{(\zeta_A^2 + 1)r_0^2 - (\zeta_B^2 - 1)}{(\zeta_A^2 + 1)r_0^2 - (\zeta_B^2 + 1)}. \end{aligned} \quad (4.13)$$

The points in the kinematic space corresponding to the above one-parameter geodesics have $0 < \alpha < \frac{\pi}{2}$, so that $\cos \alpha > 0$. The coordinates of these points are determined by the equations

$$\tan \theta = \frac{y_D}{x_D}, \quad \cos \alpha = \frac{1}{\sqrt{x_D^2 + y_D^2}} \quad (4.14)$$

Then we find a curve in the kinematic space, which is determined by the relation

$$\cos \alpha = \pm \frac{\sqrt{a^2 + b^2 + c^2 + d^2 - 2}}{|c - b|} \cos(\theta - \theta_0), \quad \tan \theta_0 = \frac{b + c}{d - a} \quad (4.15)$$

This is a timelike geodesic in the kinematic space. On the contrary, if we require that this curve is timelike, we should have

$$\frac{\sqrt{a^2 + b^2 + c^2 + d^2 - 2}}{|c - b|} > 1 \quad (4.16)$$

which is equivalent to

$$|\text{Tr} \gamma| = |a + d| > 2. \quad (4.17)$$

In other words, the element γ should be hyperbolic.

For hyperbolic and elliptic transformation γ , the eigen-geodesics are

$$(x - x_P)^2 + y^2 = x_P^2 - \frac{a - d}{c} x_P - \frac{1 - ad}{c^2} \quad (4.18)$$

Then we have

$$\begin{aligned} x_D &= \frac{2c^2 x_P}{c(a - d)x + ad - 1 + c^2}, \\ y_D &= \frac{c(a - d)x + ad - 1 - c^2}{c(a - d)x + ad - 1 + c^2}. \end{aligned} \quad (4.19)$$

In the kinematic space, the corresponding points form a geodesic, still described by Eq. (4.15). However, the geodesic is no longer timelike. Actually, for an elliptic transformation the geodesic is spacelike, while for a parabolic transformation the geodesic is null.

4.3 BTZ and kinematic space

We have showed that the horizon length L_H in the BTZ spacetime equals the geodesic distance $\Delta\tau$ in the kinematic space. In the kinematic space, for any pair of time-like separated points, it corresponds to a BTZ spacetime. On the other hand, for a fixed BTZ spacetime obtained by the identification $\{\gamma\}$ on a pair of geodesics in the Poincaré disk, it would be interesting to discuss its kinematic space. The kinematic space for the BTZ spacetime is still defined by the geodesics in the BTZ spacetime. We may start from the geodesics in the Poincaré disk, and take into account of the identification $\{\gamma\}$ on all the geodesics.

As showed in the left figure of Fig. 6, the BTZ spacetime is obtained by identifying a pair of non-intersected geodesics $\mathbf{L}_1, \mathbf{L}_2 = \gamma\mathbf{L}_1$. Between these two geodesics, there is a fundamental region. On the boundary, the two geodesics divide the boundary of the disk into four parts. We mark them as B_1, B_2, C_1, C_2 , where B_i 's are the boundaries of the fundamental region, corresponding to the two boundaries of the BTZ wormhole, and C_i 's are the remaining parts on the circle. Then we can label any geodesic in H_2 by the regions where its two endpoints locate. For example, a geodesic with one endpoint in B_1 and the other in C_2 is labelled by B_1C_2 or C_2B_1 . Note that the order in the label represents the orientation: B_1C_2 means the geodesics have a starting point in B_1 and an ending point in C_2 . Here we should notice that a geodesic with the parameter (α, θ) has the starting point at $\mu = \theta - \alpha$ and the ending point at $\nu = \theta + \alpha$.

As the BTZ spacetime is a quotient of AdS_3 under the action of a Fuchsian group Γ , its kinematic space cannot be the same as the one of AdS_3 . If two points in the kinematic space of AdS_3 can be transformed to each other under the action of an element in the Γ , they represent the same geodesic in the BTZ spacetime. We would like to find the fundamental region in the kinematic space of AdS_3 , corresponding to the BTZ black hole. Here "fundamental" means that each geodesic with orientation in the BTZ spacetime has and only has one corresponding point in that region. Since there are many different points representing the same geodesic up to identification, there is ambiguity in choosing the fundamental region. Here, we give a universal rule based on the two identified geodesics defining the fundamental region in the Poincaré disk.

As shown in the right figure of Fig. 6, the kinematic space can be separated into 20 regions by the geodesics with different ending points and orientations. Note that if we reverse the orientations of the \mathbf{L}_1 and \mathbf{L}_2 simultaneously, the identification of them leads to the same BTZ black hole. We label the points corresponding to the geodesics with opposite orientation to \mathbf{L}_1 and \mathbf{L}_2 as $\bar{\mathbf{L}}_1$ and $\bar{\mathbf{L}}_2$.

There are two fixed points under the action $\Gamma = \{\gamma\}$, as shown in the left figure of Fig. 6 which are the intersection point between the orange geodesic and the boundary. They lie on the boundaries C_1 and C_2 , labelled by f_1 and f_2 . They divide the boundaries C_1 and C_2 into two parts respectively. The fundamental region for the BTZ spacetime

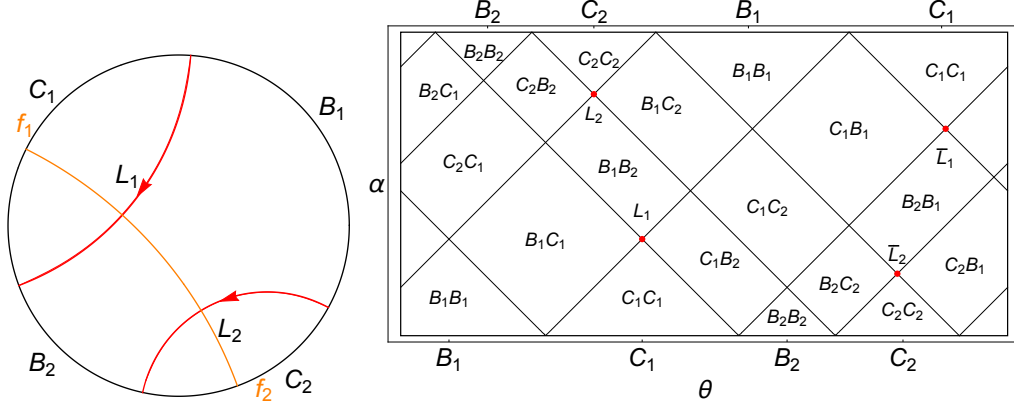


Figure 6: On the left, we draw the four regions on the boundary of Poincaré disk which are divided by the two oriented red geodesics identified with each other. The orange line is the horizon, and its two endpoints on the boundary is the fixed points of the corresponding transformation. On the right, we separate the whole kinematic space into 20 regions and marked them by the starting point and ending point of the corresponding geodesics.

in the Poincaré disk is the region between two geodesics L_1 and L_2 with two boundaries B_1 and B_2 . Under the action of γ , the fundamental region is transformed to the region with the boundaries in C_1 next to B_1 and B_2 . Similarly the action of γ^{-1} transforms the fundamental region to the region with the boundaries in C_2 next to B_1 and B_2 . Furthermore all the regions under action of $\gamma^n, n \in \mathbb{Z}$ on the fundamental region cover the whole Poincaré disk.

On the other hand, each geodesics in the Poincaré disk can be related to the one in the BTZ spacetime by the action of Γ . If the ending point of the geodesic in the disc is in C_i , it can always be mapped to the point in B_i . However, the resulting geodesic in the BTZ spacetime may wind around the horizon. In order to classify the geodesics in the BTZ spacetime, we need to consider the action of the Fuchsian group more carefully.

To discuss the action of the Fuchsian group on the geodesics in the disk, we start from the geodesics with at least one ending point being the fixed point and study the action of Γ on them. Actually, as any point on the boundary can be mapped to the fixed point by the continual action of the fundamental element γ , all the geodesics on the Poincaré disk can be related to the geodesics ending at the fixed point. In other words, starting from the geodesics ending at the fixed point and consider its images under the action of the element $\gamma^n, n \in \mathbb{Z}$, these images constitutes a line in the kinematic space, starting and ending at two fixed points. Moreover, each fixed point with the angular coordinate θ actually corresponds to two points with the coordinates $(\theta, 0)$ and $(\theta + \pi, \pi)$ on the boundary of the kinematic space. Therefore, as shown in Fig. 7, there are various lines, connecting two of the fixed points. Among all the lines, there are a few special ones, which are drawn in colored lines in Fig. 7.

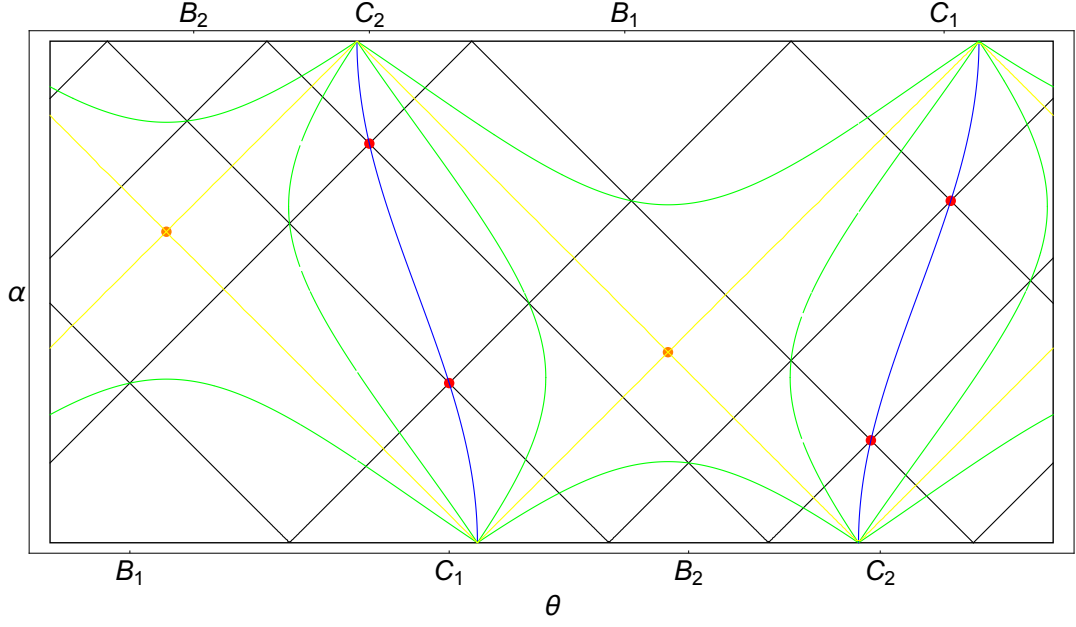


Figure 7: The blue lines are the timelike geodesic corresponding to Γ , and the corresponding geodesics in \mathbb{H}_2 are the eigen-geodesics of Γ . The points on yellow lines represent the geodesics with one endpoint being the fixed point of Γ , and having infinite windings around the horizon. The orange intersection points of two yellow lines correspond to the geodesic covering the horizon of the BTZ black hole. The points on the green lines represent the geodesics with two endpoints having the same angular coordinate and winding the horizon once.

The blue lines represent all the eigen-geodesics of γ , and the red points on it represent the geodesics \mathbf{L}_1 , \mathbf{L}_2 , $\bar{\mathbf{L}}_1$ and $\bar{\mathbf{L}}_2$ respectively. These geodesics represent the radial direction, all the points on the same geodesic having the same angular coordinate. Moreover, the blue lines themselves are also geodesic in the kinematic space.

The points on yellow lines represent all the geodesics with one endpoint being the fixed point and having infinite windings around the horizon. The two intersection points between the yellow lines represent the geodesic connecting the two fixed points on the boundaries of \mathbb{H}_2 . The geodesic actually covers the horizon of the BTZ wormhole. If the point in the kinematic space is timelike separated from the intersection points, then the corresponding geodesic does not intersect with the horizon and its endpoints are on the same boundary. And if the point is spacelike separated from the intersection point, then the corresponding geodesic does intersect with the horizon and so its endpoints are on different boundaries. Thus, the yellow lines separate all geodesics into the ones with two endpoints on the same boundary and those on different boundaries.

The points on the green lines correspond to the geodesics for which one of its endpoint can be mapped into the other by the fundamental transformation γ . Or in other words, such geodesics wind around the horizon once. Therefore the green lines separate all geodesics into the ones with or without the winding around the horizon. The points in the regions between the two timelike green lines containing the blue lines correspond to the geodesics without winding and with the endings on different boundaries. The points in the regions between the spacelike green lines and the boundary of kinematic space correspond to the geodesics without winding and with the endings on the same boundary. The points in the regions between all the green lines containing the yellow lines correspond to the geodesics with windings on the horizon, and the yellow lines divide them into the ones ending on different boundaries or on the same boundary.

Now we can determine the fundamental region of the BTZ wormhole in the kinematic space. The points in the regions B_1B_1 and B_2B_2 represent the geodesics ending on the same boundary, and the ones in B_1B_2 represent the geodesics ending on different boundaries, and all of them correspond to the geodesics without winding. For a point in the region C_1C_1 , C_2C_2 or C_1C_2 , we can always find an element in Γ which transforms at least one endpoint of the corresponding geodesic into B_i . So the regions C_iC_j will not be included into the fundamental region. Then the main question is focused on the regions B_iC_j and C_jB_i . Since the geodesics corresponding to the points in these two regions differ only on orientation, we discuss only B_iC_j below. For every geodesic in B_iC_2 we can always find an element in Γ which transforms the endpoint in B_i to C_1 and the other endpoint in C_2 to B_i , we just need to choose the regions C_1B_i and B_iC_1 , or the regions C_2B_i and B_iC_2 , to be part of the fundamental region. For the former choice, the corresponding fundamental region is drawn in blue in the left figure of Fig. 8. This is similar as the choice in Fig.17 of [7], but with a little difference because they ignore the orientation. For the latter choice, the fundamental region is drawn in yellow

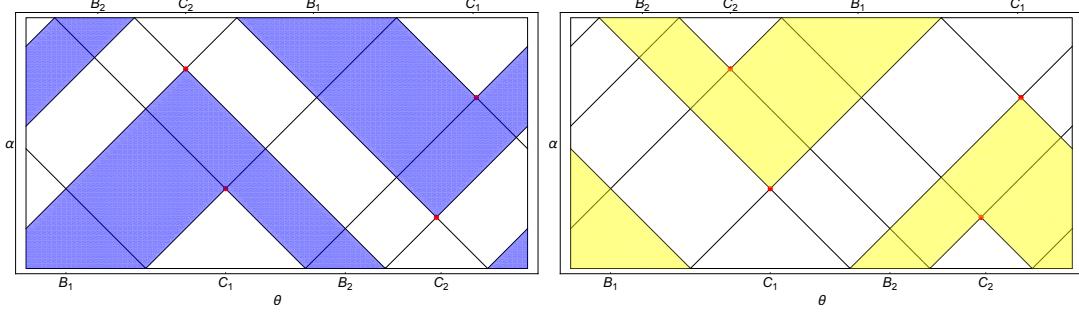


Figure 8: Two different choices for the fundamental regions for a BTZ wormhole. On the left we include the regions $B_i C_1$ and $C_1 B_i$, and on the right we include the regions $B_i C_2$ and $C_2 B_i$ instead. Both of them includes the $B_i B_j$ regions. We define the left figure corresponding to the identification $\mathbf{L}_2 = \gamma \mathbf{L}_1$, and the right figure corresponding to the identification $\bar{\mathbf{L}}_1 = \gamma^{-1} \bar{\mathbf{L}}_2$.

in the right figure of Fig. 8.

Here we make a rule for the choice, which will be used in the discussion of multi-boundary wormhole. If the Fuchsian group we choose is generated by γ , $G = \{\gamma\}$, with $\mathbf{L}_2 = \gamma \mathbf{L}_1$, then we choose the fundamental region to include $C_1 B_i$ and $B_i C_1$. But if the Fuchsian group we choose is generated by γ^{-1} , $G = \{\gamma^{-1}\}$, with $\bar{\mathbf{L}}_1 = \gamma^{-1} \bar{\mathbf{L}}_2$, then we choose the fundamental region to include $C_2 B_i$ and $B_i C_2$. Actually, both choices correspond to the same wormhole with the same identification, we make this rule just for self-consistent discussion. It does not make any difference if we choose an opposite rule.

4.4 Multi-boundary wormhole in kinematic space

For a three-boundary wormhole and a torus wormhole, both are defined by the identifications of two pairs of geodesics. The identifications are generated by two fundamental elements γ_1, γ_2 of the corresponding Fuchsian group $\Gamma = \{\gamma_1, \gamma_2\}$. We denote the four geodesics as $\mathbf{L}_{i,j}$ with $\mathbf{L}_{i,2} = \gamma_i \mathbf{L}_{i,1}, i = 1, 2$. The geodesics and the boundaries in the Poincaré disk are shown in the left figure of Fig. 9. In this figure, we choose the identification to get a three-boundary wormhole. The discussion for other identification is similar. Now the geodesics on the Poincaré disk can be classified into 72 classes, depending on their ending points. Correspondingly, the kinematic space is separated into 72 regions.

Now let us discuss the fundamental region for this three-boundary wormhole. Notice that each pair of identified geodesics $\mathbf{L}_{i,1}, \mathbf{L}_{i,2}$ can define a BTZ spacetime corresponding to γ_i such that $\mathbf{L}_{i,2} = \gamma_i \mathbf{L}_{i,1}$, and we can read the fundamental region for the resulting BTZ according to the rule we defined above. Since any points outside this fundamental region can be mapped into it by an element γ_i^n , then the regions including those points

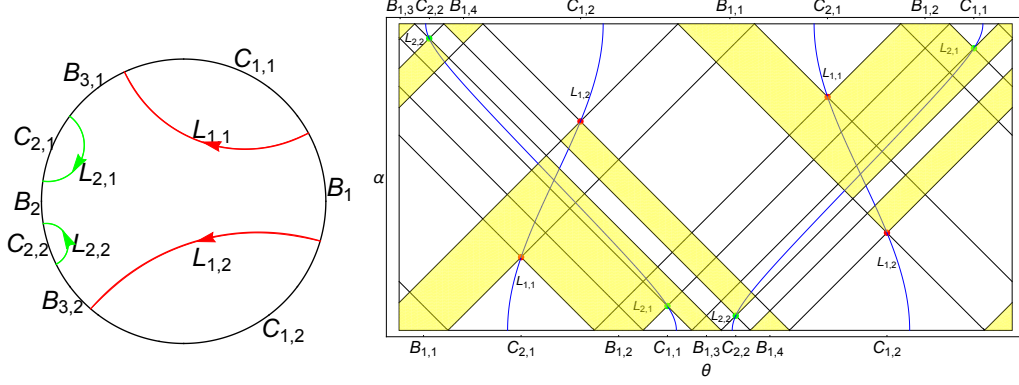


Figure 9: Three-boundary wormhole and its fundamental region in the kinematic space. In the left figure, the two pairs of identified geodesics are shown in Poincaré disk, and they divided the boundary into eight regions. In the right figure, the fundamental region in the kinematic space is shown. The red and green points correspond to the identified geodesics, and the blue lines are the timelike geodesics formed by eigen-geodesics of γ_1, γ_2 .

must not be a part of the fundamental region for the wormhole. So the fundamental region of a three-boundary wormhole, as shown in the right figure of Fig. 9, is the intersection of the fundamental regions of all the BTZ defined by each pair of geodesics. And this way to choose the fundamental region works for all kinds of multi-boundary wormhole.

As we mentioned above, for the same four geodesics a different kind of identification leads to a single-boundary torus wormhole. As showed in the upper half of Fig. 10, the geodesics in the same color are identified. We should notice that the fundamental region in this identification is the same as the three-boundary wormhole in Fig. 9. This is just because we choose the group to be generated by γ_1, γ_2 . If we choose the generators to be γ_1, γ_2^{-1} , the fundamental region is showed in the lower half of Fig. 10. Although the fundamental region may be the same for different kinds of wormhole, the same point corresponds to different kinds of geodesics in these wormholes, since the identification is different.

In order to distinguish different kinds of wormholes, it is not enough to consider only the fundamental region, which is determined by the fundamental elements in the Fuchsian group. We need to take the exact identification into account. One simple way to do this is to draw the geodesics corresponding to the fundamental elements clearly. For example, the fundamental region in yellow in the upper of Fig. 10 looks the same as the one in Fig. 9. However, the geodesics characterizing the identifications γ_i are obviously different.

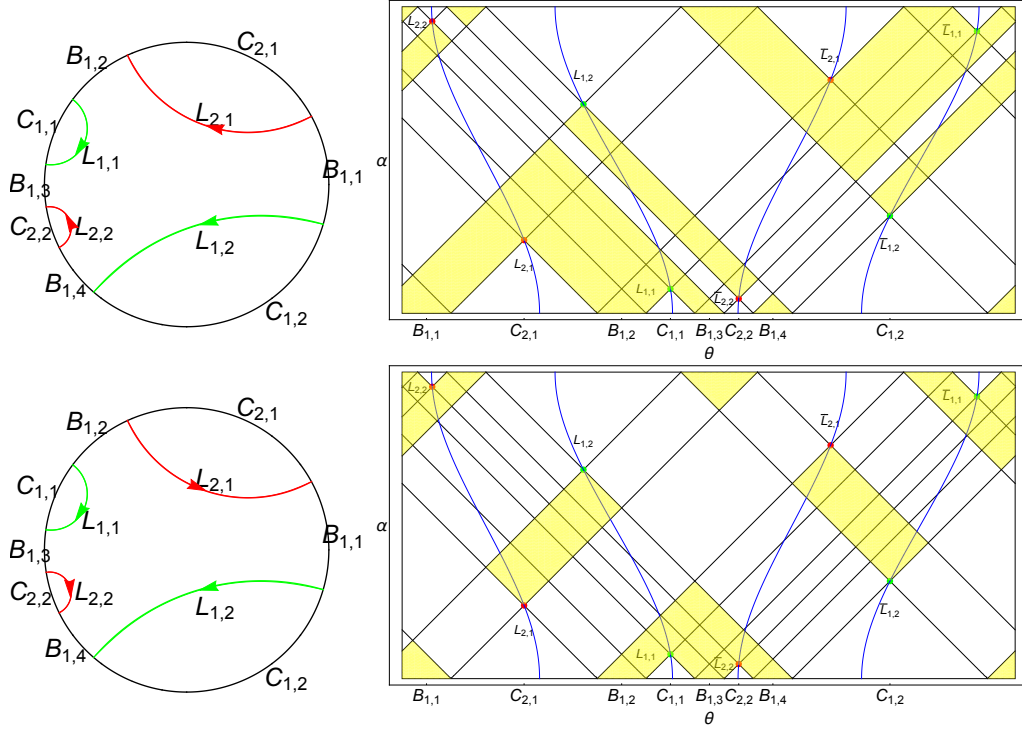


Figure 10: Single-boundary torus wormhole and its fundamental region in the kinematic space for $\Gamma = \gamma_1, \gamma_2$ is shown on the upper half part. In the left figure, the two pairs of identified geodesics are shown in Poincaré disk, and they divided the boundary into eight regions. In the right figure, the fundamental region in the kinematic space is shown. The red and green points correspond to the identified geodesics, and the blue lines are the timelike geodesics formed by eigen-geodesics of γ_1, γ_2 . On the lower half part, the same wormhole but the group is generated differently $\Gamma = \gamma_1, \gamma_2^{-1}$. In the left figure, the direction of the red geodesics are changed, suggesting the element is γ_2^{-1} .

5 Conclusion and discussion

In this paper, we studied the properties of the kinematic space from geometric points of view. First of all we showed how the kinematic space of AdS_3 can be constructed geometrically in the embedding space. As every geodesic on the Poincaré disk is the boundary of the intersection between the Poincaré disk and another disk centered outside, the kinematic space is actually formed by the tip points of the causal diamond of the other disk in the embedding space. In this picture, the causal structure in the kinematic space is easily understood. Moreover we discussed the Fuchsian group and its action on the geodesics to get the multi-boundary wormhole. We showed that for each $SL(2, R)$ transformation in the Fuchsian group its eigen-geodesics make up a geodesic in the kinematic space. If the transformation is hyperbolic, elliptic or parabolic, the corresponding geodesic in the kinematic space is timelike, spacelike or null respectively. More surprisingly, the horizon length of the BTZ wormhole can be read by the length of the corresponding timelike geodesic in the kinematic space. Finally we discussed the kinematic space for the multi-boundary wormhole. We started from the kinematic space for global AdS_3 and considered the identification of the elements in the Fuchsian group. For the BTZ blackhole, we defined consistently its fundamental region in the kinematic space. For the three-boundary wormhole, we argued that its fundamental region in the kinematic space is formed by the intersection of two fundamental regions of the BTZ wormhole constructed by two fundamental elements in its Fuchsian group. For the single-boundary wormhole, its fundamental region could be same as the one for the three-boundary wormhole, but the timelike geodesics corresponding to the identification are different.

Our study on the kinematic space is purely geometrical, having nothing to do with the differential entropy. The discussion is quite different from the ones in the literature. Our approach could be applied to the study of the holographic entanglement entropy and bit threads[27]. We would like to leave them for future study[28].

Acknowledgments

The work was in part supported by NSFC Grant No. 11275010, No. 11335012 and No. 11325522. We would like to thank B. Czech and M. Headrick for helpful discussions.

References

- [1] S. Ryu and T. Takayanagi, “Holographic derivation of entanglement entropy from AdS/CFT ,” *Phys. Rev. Lett.* **96**, 181602 (2006) [[hep-th/0603001](#)].

- [2] S. Ryu and T. Takayanagi, “Aspects of Holographic Entanglement Entropy,” JHEP **0608**, 045 (2006) [hep-th/0605073].
- [3] A. Lewkowycz and J. Maldacena, “Generalized gravitational entropy,” JHEP **1308**, 090 (2013) [arXiv:1304.4926 [hep-th]].
- [4] B. Swingle, “Entanglement Renormalization and Holography,” Phys. Rev. D **86**, 065007 (2012) [arXiv:0905.1317 [cond-mat.str-el]].
- [5] M. Van Raamsdonk, “Building up spacetime with quantum entanglement,” Gen. Rel. Grav. **42**, 2323 (2010) [arXiv:1005.3035 [hep-th]].
- [6] F. Pastawski, B. Yoshida, D. Harlow and J. Preskill, “Holographic quantum error-correcting codes: Toy models for the bulk/boundary correspondence,” JHEP **1506**, 149 (2015) [arXiv:1503.06237 [hep-th]].
- [7] B. Czech, L. Lamprou, S. McCandlish and J. Sully, “Tensor Networks from Kinematic Space,” arXiv:1512.01548 [hep-th].
- [8] B. Czech, G. Evenbly, L. Lamprou, S. McCandlish, X. L. Qi, J. Sully and G. Vidal, “A tensor network quotient takes the vacuum to the thermal state,” arXiv:1510.07637 [cond-mat.str-el].
- [9] P. Hayden, S. Nezami, X. L. Qi, N. Thomas, M. Walter and Z. Yang, “Holographic duality from random tensor networks,” arXiv:1601.01694 [hep-th].
- [10] A. Bhattacharyya, Z. S. Gao, L. Y. Hung and S. N. Liu, “Exploring the Tensor Networks/AdS Correspondence,” arXiv:1606.00621 [hep-th].
- [11] V. Balasubramanian, B. Czech, B. D. Chowdhury and J. de Boer, “The entropy of a hole in spacetime,” JHEP **1310**, 220 (2013) [arXiv:1305.0856 [hep-th]].
V. Balasubramanian, B. D. Chowdhury, B. Czech, J. de Boer and M. P. Heller, “Bulk curves from boundary data in holography,” Phys. Rev. D **89**, no. 8, 086004 (2014) [arXiv:1310.4204 [hep-th]].
R. C. Myers, J. Rao and S. Sugishita, “Holographic Holes in Higher Dimensions,” JHEP **1406**, 044 (2014) [arXiv:1403.3416 [hep-th]].
B. Chen and J. Long, “Strong Subadditivity and Emergent Surface,” Phys. Rev. D **90**, no. 6, 066012 (2014) [arXiv:1405.4684 [hep-th]].
B. Czech, X. Dong and J. Sully, “Holographic Reconstruction of General Bulk Surfaces,” JHEP **1411**, 015 (2014) [arXiv:1406.4889 [hep-th]].
M. Headrick, R. C. Myers and J. Wien, “Holographic Holes and Differential Entropy,” JHEP **1410**, 149 (2014) [arXiv:1408.4770 [hep-th]].
B. Czech and L. Lamprou, “Holographic definition of points and distances,” Phys.

- Rev. D **90**, 106005 (2014) [arXiv:1409.4473 [hep-th]].
- B. Czech, P. Hayden, N. Lashkari and B. Swingle, “The Information Theoretic Interpretation of the Length of a Curve,” JHEP **1506**, 157 (2015) [arXiv:1410.1540 [hep-th]].
- [12] B. Czech, L. Lamprou, S. McCandlish and J. Sully, “Integral Geometry and Holography,” JHEP **1510**, 175 (2015) [arXiv:1505.05515 [hep-th]].
- [13] Gil. Solanes, “Integral geometry and curvature integrals in hyperbolic space,” Ph.D. thesis, Universitat Autònoma de Barcelona (2003).
- [14] X. Huang and F. L. Lin, “Entanglement renormalization and integral geometry,” JHEP **1512**, 081 (2015) [arXiv:1507.04633 [hep-th]].
- [15] C. T. Asplund, N. Callebaut and C. Zukowski, “Equivalence of Emergent de Sitter Spaces from Conformal Field Theory,” arXiv:1604.02687 [hep-th].
- [16] J. de Boer, F. M. Haehl, M. P. Heller and R. C. Myers, “Entanglement, Holography and Causal Diamonds,” arXiv:1606.03307 [hep-th].
- [17] M. Banados, C. Teitelboim and J. Zanelli, “The Black hole in three-dimensional space-time,” Phys. Rev. Lett. **69**, 1849 (1992) [hep-th/9204099].
- [18] M. Banados, M. Henneaux, C. Teitelboim and J. Zanelli, “Geometry of the (2+1) black hole,” Phys. Rev. D **48**, 1506 (1993) Erratum: [Phys. Rev. D **88**, 069902 (2013)] [gr-qc/9302012].
- [19] J. M. Maldacena, “Eternal black holes in anti-de Sitter,” JHEP **0304**, 021 (2003) [hep-th/0106112].
- [20] S. Aminneborg, I. Bengtsson, D. Brill, S. Holst and P. Peldan, “Black holes and wormholes in (2+1)-dimensions,” Class. Quant. Grav. **15**, 627 (1998) [gr-qc/9707036].
- [21] D. Brill, “Black holes and wormholes in (2+1)-dimensions,” Lect. Notes Phys. **537**, 143 (2000) [gr-qc/9904083].
- [22] K. Krasnov, “Holography and Riemann surfaces,” Adv. Theor. Math. Phys. **4**, 929 (2000) [hep-th/0005106].
- [23] K. Skenderis and B. C. van Rees, “Holography and wormholes in 2+1 dimensions,” Commun. Math. Phys. **301**, 583 (2011) [arXiv:0912.2090 [hep-th]].
- [24] V. Balasubramanian, P. Hayden, A. Maloney, D. Marolf and S. F. Ross, “Multi-boundary Wormholes and Holographic Entanglement,” Class. Quant. Grav. **31**, 185015 (2014) [arXiv:1406.2663 [hep-th]].

- [25] D. Marolf, H. Maxfield, A. Peach and S. F. Ross, “Hot multiboundary wormholes from bipartite entanglement,” *Class. Quant. Grav.* **32**, no. 21, 215006 (2015) [arXiv:1506.04128 [hep-th]].
- [26] H. Maxfield, “Entanglement entropy in three dimensional gravity,” *JHEP* **1504**, 031 (2015) [arXiv:1412.0687 [hep-th]].
- [27] M. Freedman and M. Headrick, “Bit threads and holographic entanglement,” arXiv:1604.00354 [hep-th].
- [28] J.d. Zhang and B. Chen, work in progress.